Research in Astronomy and Astrophysics, 23:055007 (12pp), 2023 May https://doi.org/10.1088/1674-4527/acb9da

Hybrid Optimization Algorithm in the Photometric Inversion of Periods for Asteroids

Xin-Ran Li[1,3], Yong-Xiong Zhang[2], Hai-Bin Zhao[3,4], Xiaoping Zhang[1], and Xiao-Ping Lu[1,2]
[1] State Key Laboratory of Lunar and Planetary Sciences, Macau University of Science and Technology, Macau 999078, China
[2] School of Computer Science and Engineering, Macau University of Science and Technology, Taipa, Macao 999078, China
[3] Key Laboratory of Planetary Sciences, Purple Mountain Observatory, CAS, Nanjing 210023, China; meteorzh@pmo.ac.cn
[4] CAS Center for Excellence in Comparative Planetology, CAS, Hefei 230026, China
Received 2022 November 29; revised 2023 January 5; accepted 2023 January 23; published 2023 April 19

Abstract

Asteroids, as the primitive building blocks for the formation of our solar system, could reveal its evolution mechanism, and have attracted more and more attention from the public and professional institutions in recent years. Their physical properties, such as rotational period, spin axis and overall shape, can be inverted from ground- and space-based photometric observations. Since the inversion process is very time-consuming, this paper combines the genetic algorithm with the Levenberg–Marquardt (LM) algorithm, and presents a hybrid optimization algorithm based on a Cellinoid shape model for the inversion of rotational periods, which greatly improves the inversion efficiency. The proposed hybrid algorithm is applied to the synthetic lightcurves generated for an assumed Cellinoid shape model and the inverted rotational period results are consistent with the preset ones with a reduced search time, compared with the LM algorithm. Finally, multiple numerical experiments on the periods are performed on lightcurves and sparse observations of real asteroids to confirm that the proposed method can perform well in improving computational efficiency.

Key words: astrometry – methods: numerical – planets and satellites: fundamental parameters

1. Introduction

Asteroids can uncover the underlying information about the origin and early evolution of the solar system. Therefore, as an important part of planetary science research, asteroids in the solar system constitute one of the current hot spots in planetary sciences. So far, a majority of data used to derive asteroid parameters have usually come from the analysis of photometric observations obtained by ground-based telescopes. With the development of telescope technology, a large number of observations are collected through ground-based and space-based surveys, such as LINEAR, Pan-STARRS, and others. As most asteroids are too small and faint to be resolved by remote observation, in general, an integrated brightness is commonly used to further analyze the features of asteroids, including their rotational period, pole direction and shape.

Russell (1906) first studied the problem of determining the shape of asteroids in 1906 from their integrated brightness, and claimed that the information was not sufficient to reconstruct the shape model of asteroids from the lightcurve observed at opposition. Later, many methods for deriving physical parameters of asteroids from photometric observations have been developed that are based on observations acquired. Surdej & Surde (1978) calculated synthetic lightcurves by assuming the asteroidal shape as a triaxial ellipsoid shape for both Lambert's and Lommel-Seeliger's scattering laws. Based on the Lumme-Bowell scattering law (Lumme & Bowell 1981a, 1981b), Karttunen & Bowell (1989) proposed a method to generate lightcurves using a triaxial ellipsoid, and found that the brightness change of lightcurves largely depends on the variation of the model shape, rather than the scattering law. However, the lightcurve morphology generated by the ellipsoid model is symmetric due to its symmetrical shape. For the purpose of having a better simulation of real irregular asteroids, Cellino et al. (1989) introduced a more general shape model, which consists of eight adjacent ellipsoid octants with different semi-axes, with the constraint that adjacent octants must have two identical semi-axes.

With the improvement of computing power, more studies focused on the improvement of inverting the physical parameters of asteroids. Kaasalainen et al. (1992b, 1992a) presented an inversion method based on the convex shape model, and exploited a separable scattering function (Kaasalainen & Torppa 2001; Kaasalainen et al. 2001, 2005). Large sky survey projects tend to collect a large number of sparse observations of asteroids, making it difficult to reconstruct a complex shape model from these limited data. Cellino et al. (2009) attempted to apply the genetic algorithm (GA) to determine physical parameters of asteroids based on an ellipsoidal shape from sparse photometric data. Lu et al. (2013) introduced a numerical algorithm based on the Levenberg-Marquardt (LM) algorithm to efficiently calculate the parameters of asteroids within an ellipsoidal approximation. Furthermore, by using the asymmetric Cellinoid shape model, Lu et al. (2014) developed the inverse process from observation data in the form of lightcurve or sparse format, and applied it to Hipparcos data set, which confirmed the proposed inverse approach is effective and efficient for dealing with sparse observations (Lu et al. 2016).

As in most of inversion approaches the brightness is simulated by a surface integration based on the discretization of the assumed shape model, like convex and Cellinoid shapes, this is very time-consuming, although several outstanding works attempted to infer the theoretical formula of brightness based on the ellipsoidal shape model (Muinonen & Lumme 2015; Muinonen et al. 2015). Moreover, the optimization based on the gradient descent methods comes with a high computational cost, especially for some local optimal methods, like LM. Since the GA might obtain an approximate solution through a global search, this motivates us to propose a hybrid method that combines GA and LM methods together to reduce the huge computational cost when inverting parameters, especially for a large number of observation data. Actually, mixing multiple optimization algorithms to search the optimal solution from high-dimensional parameter space has become a common choice in practice (Cho & Zhang 2004; Peňa et al. 2004; Li et al. 2019).

This paper is organized as follows. In Section 2 the Cellinoid shape model and its inverse process are briefly described. Followed is the introduction of GA and LM algorithms, as well as the proposed hybrid method in Section 3. Then Section 4 shows the experimental results of the new proposed method, applied to both synthetic and real observations in lightcurve and sparse format. Finally the conclusions are drawn in Section 5.

2. Cellinoid Shape Model

The Cellinoid shape model employed in this article is shown in Figure 1, whose mass can be calculated by

$$M = \frac{\rho\pi}{6}(a_1 + a_2)(b_1 + b_2)(c_1 + c_2), \tag{1}$$

with the assumption that the volume density ρ is uniform, as well as the center by

$$\vec{G} = \begin{pmatrix} \bar{x} \\ \bar{y} \\ \bar{z} \end{pmatrix} = \begin{pmatrix} \frac{3}{8}(a_1 - a_2) \\ \frac{3}{8}(b_1 - b_2) \\ \frac{3}{8}(c_1 - c_2) \end{pmatrix}. \tag{2}$$

Since the Cellinoid shape model is asymmetric, its center of mass varies with respect to the origin of the coordinate system. As introduced by Lu et al. (2014), a rigid body will rotate stably about the axis of maximum moment of inertia. Supposing moment of inertia I_O rotating about the line with a unit direction vector $\boldsymbol{\eta}$ and passing through the origin O can be calculated as

$$I_O = I_G + M\bar{r}^2, \tag{3}$$

where I_G is the moment of inertia rotating about the line with the direction $\boldsymbol{\eta}$ and passing through the center of mass G of the Cellinoid. The distance $\bar{r}$ can be obtained with $\bar{r}^2 = \boldsymbol{\eta}^T B\boldsymbol{\eta}$. The moment of inertia I_O has the form

$$I_O = \iiint |\overrightarrow{OM} \times \boldsymbol{\eta}|\rho dV = \boldsymbol{\eta}^T A\boldsymbol{\eta}, \tag{4}$$

where $\overrightarrow{OM}$ is the vector between the origin and an arbitrary point in the Cellinoid. Then the moment of inertia I_G passing the center of mass will be derived as $I_G = \boldsymbol{\eta}^T(A - MB)\boldsymbol{\eta}$, that is, its free rotational axis can be derived by diagonalizing the matrix $C = A - M * B$, where A and B are defined as follows,

$$A = \begin{pmatrix} I_{xx} & I_{xy} & I_{xz} \\ I_{xy} & I_{yy} & I_{yz} \\ I_{xz} & I_{yz} & I_{zz} \end{pmatrix},$$
$$B = \begin{pmatrix} \bar{y}^2 + \bar{z}^2 & -\bar{x}\bar{y} & -\bar{x}\bar{z} \\ -\bar{x}\bar{y} & \bar{x}^2 + \bar{z}^2 & -\bar{y}\bar{z} \\ -\bar{x}\bar{z} & -\bar{y}\bar{z} & \bar{x}^2 + \bar{y}^2 \end{pmatrix}. \tag{5}$$

The form of the elements in A is given as follows,

$$I_{xx} = \iiint (y^2 + z^2)dV \tag{6}$$

$$\begin{aligned} &= \frac{\pi}{30}[(a_1 + a_2)(b_1^3 + b_2^3)(c_1 + c_2) \\ &\quad + (a_1 + a_2)(b_1 + b_2)(c_1^3 + c_2^3)], \\ I_{xy} &= -\iiint (xy)dV = -\frac{1}{15}(a_1^2 - a_2^2)(b_1^2 - b_2^2)(c_1 + c_2). \end{aligned} \tag{7}$$

Since the disk-integrated brightness is not sensitive to the geometric albedo on the surface of asteroids and generally the albedo distribution of asteroids varied little, a linear combination of the Lambert and Lommel-Seeliger functions presented by Kaasalainen et al. (2001) is exploited to simulate the surface scattering law,

$$S(\mu, \mu_0, \alpha) = f(\alpha)\left(\frac{\mu\mu_0}{\mu + \mu_0} + \gamma\mu\mu_0\right), \tag{8}$$

where γ is a partition factor between the single and multiple scattering laws, and $f(\alpha)$ is a four-parameter empirical surface phase function first proposed by Muinonen et al. (2002),

$$f(\alpha) = A\exp\left(-\frac{\alpha}{D}\right) + B + K\alpha, \tag{9}$$

where α is the phase angle. In addition, μ and μ_0 are defined as

$$\mu = \eta \cdot E, \qquad \mu_0 = \eta \cdot E_0, \tag{10}$$

where η denotes the outward unit normal vector of the surface. E and E_0 represent directions to the Earth and the Sun as observed from the asteroid, respectively. The exponential part in the phase function can better simulate the opposition effect as the solar phase angle is close to 0. While the observations for most of main belt asteroids are larger than 10°, the exponential part in the scattering function could be ignored to reduce the complexity. Finally, the total number of parameters in the Cellinoid shape model is thus 13, namely six parameters for shaping the asteroid (a_1, a_2, b_1, b_2, c_1, c_2), the pole direction (λ, β) in ecliptic coordinate system, the rotational period P with the initial rotational phase angle Φ_0, and three scattering parameters (γ, B, K).

Here it should be noted that in the inversion process we always fix the first semi-axis (i.e., a_1) to be 1 as the shape model is only relative. This will reduce the total inverted parameters to 12 for saving the searching time. The parameters B and K in the solar phase function will scale the total brightness to fit the real observations even though the shape model is represented in relative axial ratio format. This makes the phase function differ from the version used in Kaasalainen et al. (2001), where the parameter B is set to 1.

Following the definition of scattering function in Equation (8), the observed brightness of a given asteroid under a specific viewing geometry can be simulated by the surface integration,

$$L(\omega_0, \omega) = \int\int_{C+} S(\mu, \mu_0, \alpha) d\sigma, \tag{11}$$

where $C+$ is the fraction of illuminated surface that is visible to the observer, i.e., $\mu > 0$, $\mu_0 > 0$. Supposing the shape model is a Cellinoid, then by applying triangularization to each octant of the Cellinoid, the brightness integral can be discretized as,

$$L(\omega_0, \omega) \approx \sum_{i=1}^{8}\sum_{j=1}^{N} S(\mu, \mu_0, \alpha)\Delta S_{i,j}, \tag{12}$$

where i is the index of octant, j is the index of triangular facet in each octant, and $\Delta S_{i,j}$ means the area of the jth facet on the ith octant.

Then the best-fit physical parameters could be searched by minimizing the residual for relative lightcurves (Kaasalainen & Torppa 2001),

$$\chi^2 = \sum_i \| \frac{L_i}{\langle L_i \rangle} - \frac{\widetilde{L}_i}{\langle \widetilde{L}_i \rangle} \|^2, \tag{13}$$

where L_i is the observed ith lightcurve with the calibrated brightness, $\widetilde{L}_i$ is the corresponding simulated ith lightcurve.

3. Hybrid Method of GA and LM Algorithms

The optimization of relative residual (Equation (13)) is a very time-consuming process, especially applying some gradient-based optimization methods since these type methods always obtain the local optimized solutions. For obtaining the global optimized solution, a large number of initial guesses are implemented and the final solution with the smallest residual is chosen as the best-fit solution. However, heuristic methods such as the GA and particle swarm optimization (PSO), can perform well in searching the global solution while the solution accuracy obtained by these methods is not as high as the gradient-based methods.

In this section, a commonly used gradient-based method, the LM method is briefly introduced , followed by the description of one popular heuristic method, the GA method. Finally, a hybrid method that integrates the LM and GA algorithms is proposed to utilize the advantages of the two methods, i.e., try to obtain a globally optimized solution in an efficient way while preserving accuracy.

3.1. Levenberg–Marquardt (LM) Algorithm

The LM algorithm is an efficient method for solving nonlinear optimization problems, as the extension of the steepest descent method based on gradient optimization. Marquardt (1963) first proposed this method for varying smoothly between the extremes of the inverse-Hessian method and the steepest descent method. The latter method is first used as far from the minimum of the function, then the LM method switches continuously to the former as the minimum is approached. The algorithm process is summarized by Press et al. (1992) as follows,

1. Given an initial guess for the set of fitted parameters $\boldsymbol{x}$.
2. Compute $\chi^2(\boldsymbol{x})$.
3. Pick a modest value for λ.
4. (*) Solve the curvature matrix equation $\alpha\,\delta\,\boldsymbol{x} = \beta$ for $\delta\,\boldsymbol{x}$ and evaluate $\chi^2(\boldsymbol{x} + \delta\,\boldsymbol{x})$.
5. If $\chi^2(\boldsymbol{x} + \delta\,\boldsymbol{x}) \geqslant \chi^2(\boldsymbol{x})$, increase λ by a factor of 10 and go back to (*).
6. If $\chi^2(\boldsymbol{x} + \delta\,\boldsymbol{x}) < \chi^2(\boldsymbol{x})$, decrease λ by a factor of 10, update the trial solution $\boldsymbol{x}' = \boldsymbol{x} + \delta\boldsymbol{x}$ and go back to (*).

As for the stop condition in practice, it could be considered that iteration reaches the preset number, or the change of $\chi^2(\boldsymbol{x})$ decreases by a negligible amount, and also λ reaches a predetermined value.

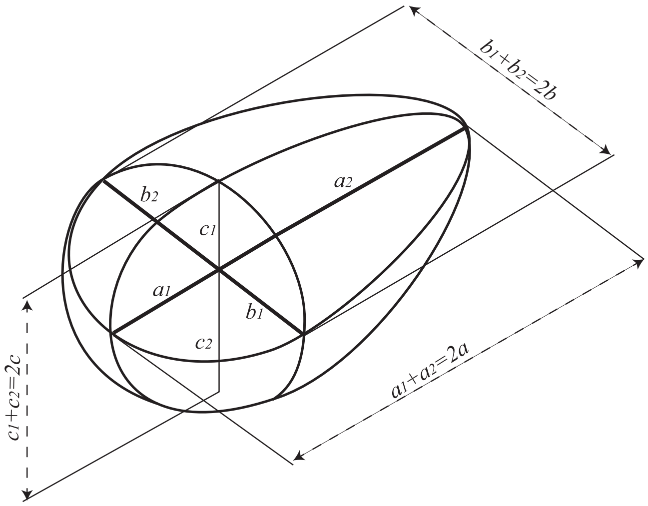

Figure 1. Cellinoid shape model.

As the Hessian matrix ($2 * \alpha$) is hard to compute and the second-derivative term makes the model unstable, the LM algorithm replaces this matrix by using a simplified formula,

$$\alpha_{kl} = \sum_{i=1}^{N}\left(\frac{\partial\chi^2}{\partial \boldsymbol{x}_k}\frac{\partial\chi^2}{\partial \boldsymbol{x}_l}\right). \tag{14}$$

For the relative residual (Equation (13)), the matrix α is complex as the synthetic lightcurve mean should be incorporated into the Hessian matrix and we list it and the gradient β here,

$$\alpha_{kl} = \sum_{i=1}^{m}\left[\sum_{j=1}^{M_i}\left(\frac{\partial}{\partial \boldsymbol{x}_k}\left(\frac{\widetilde{L}_j^{(i)}(\boldsymbol{x})}{<\widetilde{L}^{(i)}>}\right)\cdot\frac{\partial}{\partial \boldsymbol{x}_l}\left(\frac{\widetilde{L}_j^{(i)}(\boldsymbol{x})}{<\widetilde{L}^{(i)}>}\right)\right)\right], \tag{15}$$

and,

$$\beta_k = \sum_{i=1}^{m}\left[\sum_{j=1}^{M_i}\left(\left[\frac{L_j^{(i)}}{\langle L^{(i)}\rangle} - \frac{\widetilde{L}_j^{(i)}(\boldsymbol{x})}{<\widetilde{L}^{(i)}>}\right]\cdot\frac{\partial}{\partial \boldsymbol{x}_k}\left(\frac{\widetilde{L}_j^{(i)}(\boldsymbol{x})}{<\widetilde{L}^{(i)}>}\right)\right)\right], \tag{16}$$

where m denotes the total number of lightcurves and M_i denotes the data points number in each lightcurve.

3.2. Genetic Algorithm (GA)

The Genetic Algorithm, first proposed by Holland and De Jong in the 1970s (De Jong 1975; Holland 1975), is a typical heuristic method that simulates the natural selection mechanism of Darwin's biological evolution theory in order to obtain a global optimized solution.

GA encodes the solution vector of the problem as a chromosome, and each element in the solution vector is called a gene in the chromosome. By simulating the process of biological evolution, GA randomly generates chromosomes as the initial population with the specified range, and evaluates the fitness of each chromosome to measure the quality of the population based on a fitness function. The smaller the fitness value, the better the individual, that is, the closer to the optimized solution. Through genetic operations such as selection, crossover and mutation, the chromosomes can be evolved iteratively into a new population with better fitness, and can be used to obtain a best-fit solution through continuous evolution. The whole evolution process of GA is shown in Figure 2. In practice, the evolution process could be terminated as the maximum step is reached or the population fitness does not decrease.

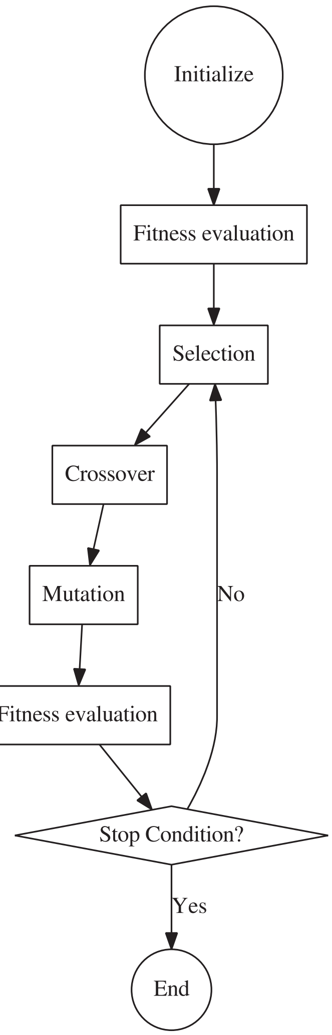

Figure 2. The flowchart of genetic algorithm.

3.3. Hybrid of GA and LM Algorithms

There are 13 parameters in total for simulating the asteroid photometric brightness. The inverse problem of fitting the 13 parameters from observations is a time-consuming problem by the gradient-based optimization method. However, the GA method cannot obtain the best-fit solution with high accuracy. Therefore, in this section a hybrid method merging the GA and LM algorithms is proposed with the purpose of accelerating the search efficiency while preserving accuracy.

Generally, the rotational period is always the first-order approximation during the inverse process, i.e., it is the first parameter to converge, which has been fully investigated and described by Kaasalainen & Torppa (2001), Lu et al. (2017). In practice, the rotational period is first searched for with an initial random guess for all the 13 parameters. After deriving the rotation period, the whole inverse process will search the remaining 12 parameters again by setting the derived estimate of period as the initial rotational period, and meanwhile the rotational period is also refined.

The new proposed hybrid method of GA and LM is actually a special optimization strategy that treats the entire LM algorithm as the fitness function in the process of GA. By taking the search of rotational period as an example, first randomly generate a set of period values as the initial population of GA. The complete LM algorithm is used in the calculation of fitness values, and χ^2 obtained by the LM algorithm is considered as the fitness value of the corresponding individual. That is, the step "Fitness evaluation" as shown in Figure 2 is implemented by the LM algorithm. Then, based on the fitness values of the individuals, the evolutionary operations in GA (selection, crossover and mutation) are performed to obtain new individuals and this loop is conducted iteratively until some stop condition is reached and the best-fit solution is derived.

In GA, selection operation is the process of selecting better individuals based on fitness values from the previous generation for reproduction. The higher the fitness, the higher the probability of being selected. Then the crossover operation uses the arithmetic crossover method (Gen & Cheng 1996), in which offspring from the selection operation are crossed over with a certain crossover probability. Finally the mutation operation has a lower probability using dynamic mutation (Gen & Cheng 1996) to allow individuals to explore new regions with a view to finding better individuals. The variation is greater in the early stages of evolution and smaller in the later stages. The algorithm also uses an elitism strategy so that populations do not degrade.

This hybrid strategy can efficiently find several regions in the parameter space with small fitness values by employing the GA algorithm, then the LM algorithm is exploited to search the local optimal solution in each region, and eventually the global optimal solution can be obtained through comparison and evolution.

4. Numerical Experiments

In this section the proposed hybrid method will be applied to the synthetic observation data to confirm its effectiveness and show its improvement in reducing the computational cost, compared with the method based on the LM algorithm alone. Subsequently, it is also applied to the cases of real asteroids with lightcurves and sparse observations. The obtained results are consistent with previously published ones.

The settings for the hybrid method are listed as follows. The initial population number in GA is set to 25, the maximum number of iterations is set to 50, and the stagnation iteration number of fitness to 15. In the part of LM, step size λ is also set as 0.001, similar to the one in Press et al. (1992) and the code stops when maximum iteration reaches 50 or the change of $\chi^2(\boldsymbol{x})$ is smaller than 10^{-10} for 40 times.

Besides, the model parameters are subject to the following constraints: the six semi-axes of the Cellinoid shape model should satisfy $a_1 + a_2 \geqslant b_1 + b_2 \geqslant c_1 + c_2$, and $0 < a_2 \leqslant a_1 = 1$; while the ranges of other physical characteristics are chosen as, the pole direction $\lambda \in [0, 360°]$, $\beta \in [-90°, 90°]$; the rotational period (in hour) $P \in [0, 24]$; the initial rotational phase $\Phi_0 \in [0, 360°]$, as well as the scattering coefficients $K \in [-0.0024, -0.0012]$, $B \in [0.20, 0.49]$, and $\gamma \in [0.05, 0.19]$.

4.1. Application to Synthetic Lightcurves

First, in order to examine the performance of the proposed hybrid method, some synthetic lightcurves are generated using a shape model with different six semi-axes a_1, a_2, b_1, b_2, c_1 and c_2, as well as the other physical parameters. By applying the hybrid method to these lightcurves with the known preset parameters, it could be verified whether the inversion process can successfully obtain the correct results. Figure 3 shows the generated four lightcurves, each with 120 points, and the corresponding parameters are listed in the figure caption.

For better comparing the efficiency in searching the best-fit parameters respectively using the proposed hybrid method and the original LM algorithm, we set the searching space for the rotational period within the interval [0 hr, 24 hr] assuming no any prior information, although in practice a rough estimate for the rotation period could be fast obtained based on the Fourier analysis as handling the lightcurves data. Then with the increment of period $\Delta P = 0.001$ hr, the LM algorithm is implemented to derive the best-fit period and the hybrid method is also applied to search for the period. In Table 1, the derived periods for the four synthetic lightcurves by the two different methods are listed, as well as the corresponding χ^2 values and the total time cost (T in minutes). In the table, "P" denotes the true period, while "$P_{\rm LM}$" and "$P_{\rm G\&L}$" denote the derived periods in hours respectively by the LM method and the hybrid method.

It is apparent that the proposed hybrid method of GA and LM can largely reduce the total computational cost while it could still obtain the rotational period with a close accuracy to the one derived by the LM algorithm. Although the period results obtained by the two algorithms are different, they are considered equally valid within the error range. The χ^2 value of

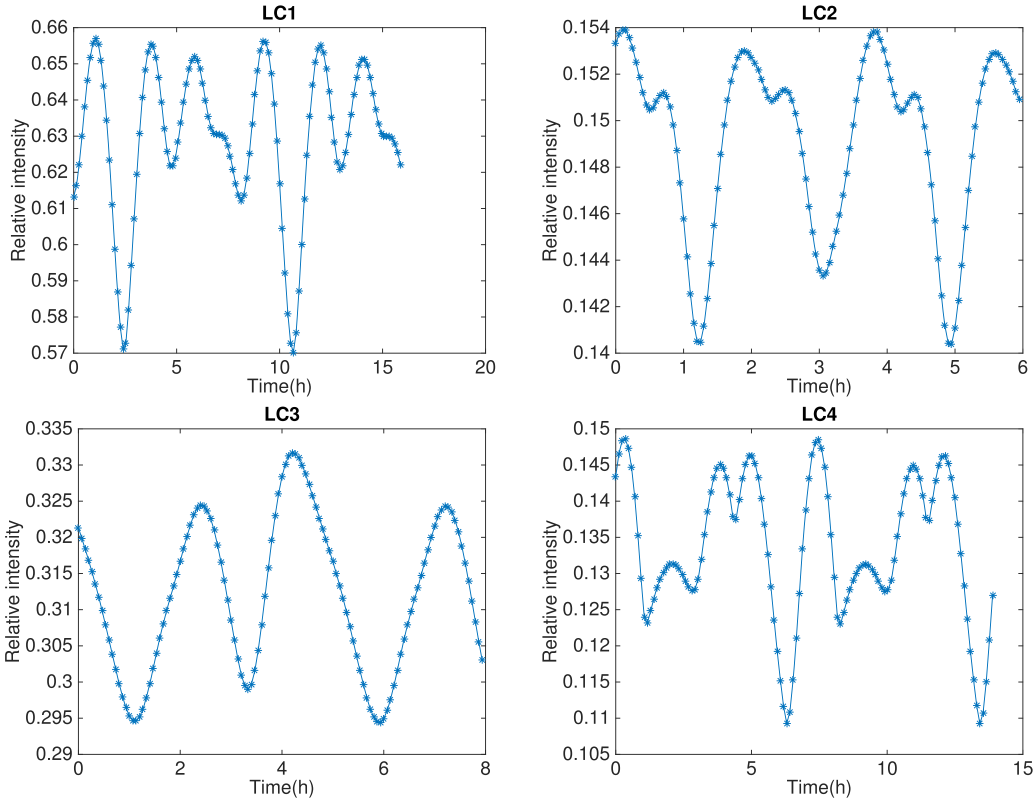

Figure 3. Synthetic lightcurves generated by the Cellinoid shapes (The parameters: LC1: $a_1 = 1.00$, $a_2 = 0.93$, $b_1 = 0.39$, $b_2 = 1.50$, $c_1 = 0.63$, $c_2 = 1.19$, $\lambda = 348.00$, $\beta = -47.00$, $P = 8.20$, $\Phi_0 = 208.00$, $K = -0.0020$, $B = 0.44$, $\gamma = 0.15$; LC2: $a_1 = 1.00$, $a_2 = 0.32$, $b_1 = 0.48$, $b_2 = 0.76$, $c_1 = 0.92$, $c_2 = 0.14$, $\lambda = 173.00$, $\beta = 11.00$, $P = 3.7$, $\Phi_0 = 43.00$, $K = -0.0023$, $B = 0.27$, $\gamma = 0.10$; LC3: $a_1 = 1.00$, $a_2 = 0.48$, $b_1 = 1.01$, $b_2 = 0.32$, $c_1 = 0.61$, $c_2 = 0.62$, $\lambda = 16.00$, $\beta = 26.00$, $P = 4.8$, $\Phi_0 = 114.00$, $K = -0.0023$, $B = 0.44$, $\gamma = 0.10$; LC4: $a_1 = 1.00$, $a_2 = 0.054631$, $b_1 = 0.65$, $b_2 = 0.26$, $c_1 = 0.29$, $c_2 = 0.56$, $\lambda = 123.00$, $\beta = -23.00$, $P = 7.12$, $\Phi_0 = 37.00$, $K = -0.0021$, $B = 0.40$, $\gamma = 0.10$.)

Table 1
Comparison of Only the LM Algorithm and the Hybrid Algorithm ($G\&L$) in the Case of Noiseless Data

LC	P/(hr)	$P_{\rm LM}$/(hr)	$P_{\rm G\&L}$/(hr)	$\chi^2_{\rm LM}$	$\chi^2_{\rm G\&L}$	$T_{\rm LM}$/(min)	$T_{\rm G\&L}$/(min)
#1	8.20	8.1911	8.2057	1.21282×10^{-3}	3.8473×10^{-3}	1967	86
#2	3.70	3.7028	3.7032	2.078×10^{-5}	2.068×10^{-5}	1961	44
#3	4.80	4.8037	4.7968	1.426×10^{-5}	3.656×10^{-5}	2181	54
#4	7.12	7.1324	7.1212	1.9483×10^{-4}	2.9×10^{-8}	1972	93

the LM method is smaller than the one of hybrid method, showing that the LM could have much higher accuracy compared to the hybrid method with GA. Certainly, the selection of the initial random parameters and the subsequent optimization of the other 12 parameters also have an effect on the final results in the LM method. Different initial parameters will lead to slight difference in the final results.

Moreover, as the increment ΔP in applying the LM algorithm decreases for obtaining a higher accuracy of the derived period, its total computational cost will be significantly enlarged. In this case, the hybrid method will show an effective way to largely reduce the total computing cost. Furthermore, the proposed hybrid method could also be applied to provide an appropriate estimate for the rotational period first and the LM method could be further used to refine it if the rotational period with higher accuracy is required.

Besides, the hybrid method does not always perform with lower accuracy than the LM algorithm. In some special cases such as the LC4 as shown in Table 1, the hybrid method almost obtains the exact correct value as same as the true period. This is because the GA method has the operation of mutation which could make the solution jump to the global optimal solution with a small probability, while the LM algorithm has to search the local optimal solution within a specified subspace. Therefore, a small increment ΔP is always essential for LM searching as mentioned by Kaasalainen et al. (2001) with a

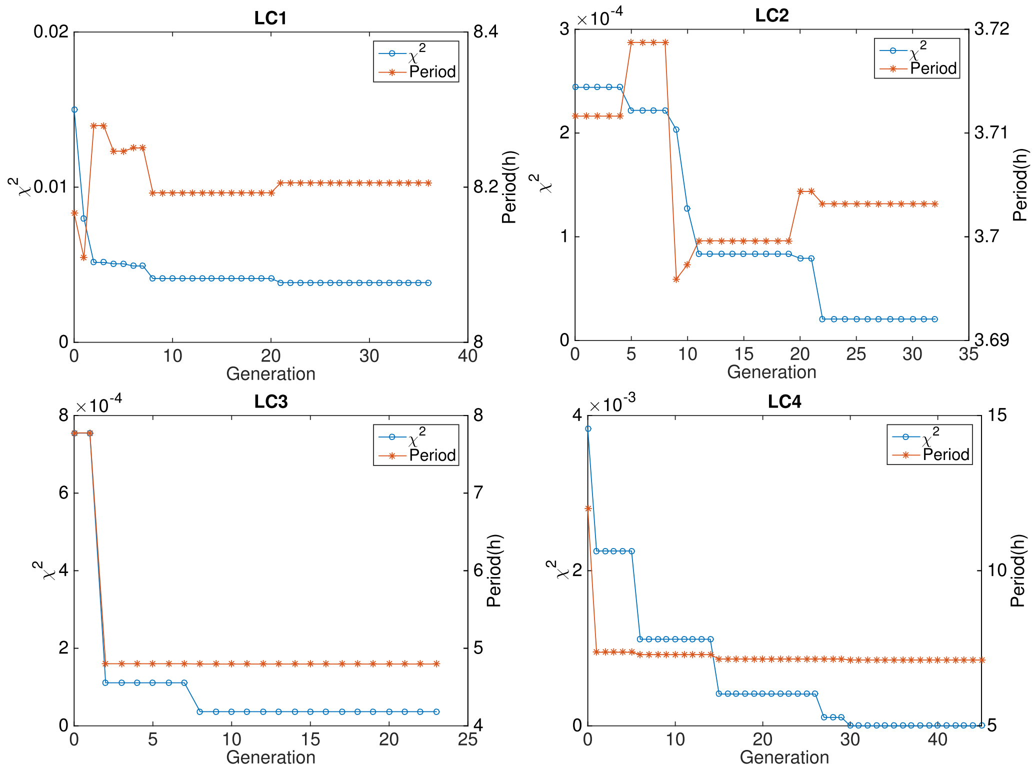

Figure 4. Convergence process of the proposed hybrid method.

suggestion about ΔP roughly given by

$$\frac{\Delta P}{P} \approx \frac{1}{2}\frac{P}{T}. \tag{17}$$

In Figure 4 the convergence process of the proposed hybrid method is presented and it is easily found that the fitness χ^2 quickly converges to the lowest value after several generations. The GA part in the hybrid method could make the whole search process more effective in approximating the global optimal solution, and meanwhile the LM algorithm can make the local search more efficient. The fusion of GA and LM can make the rotational period close to the true value after about 10 generations.

In practice, the observations are always corrupted by noise. For simulating the real observations, a 1% random Gaussian white noise $N(0,\ 0.01)$ is added to the synthetic lightcurves generated based on the Cellinoid shape models with the same parameters as shown in Figure 3. The noisy lightcurves are plotted in Figure 5, where the original synthetic lightcurves are denoted by lines while the noised observations are denoted by the stars.

Then the proposed hybrid method is applied to the noisy synthetic lightcurves and the derived best-fit rotational periods with the corresponding χ^2 as well as the time cost, are listed in Table 2. It can be found that the hybrid method can also perform well in handling the noisy observations. This is also confirmed that the rotational period is always the first-order approximation in fitting the lightcurves and the Gaussian noise on the observations will not impact the search for the rotational period too much.

Table 2
Results Derived by the Hybrid Method from Lightcurves with Gaussian Noise

LC	$P/(\mathrm{hr})$	$P_{\mathrm{G\&L}}/(\mathrm{hr})$	$\chi^2_{\mathrm{G\&L}}$	$T_{\mathrm{G\&L}}/(\mathrm{min})$
#1	8.20	8.1912	5.621×10^{-3}	83
#2	3.70	3.6922	2.686×10^{-4}	55
#3	4.80	4.7964	1.445×10^{-3}	65
#4	7.12	7.1129	3.427×10^{-4}	126

4.2. Application to Real Asteroids

The experiments for synthetic lightcurves confirm that the proposed hybrid method of GA and LM algorithms can perform effectively in accelerating the search of rotational periods and the derived optimal solutions can have a high accuracy. Then the hybrid method is applied to the observations from three real asteroids, (107) Camilla, (54) Alexandra and (16) Psyche, whose three lightcurves were observed respectively on 2004 November 6 (Hanuš et al. 2016), 2009

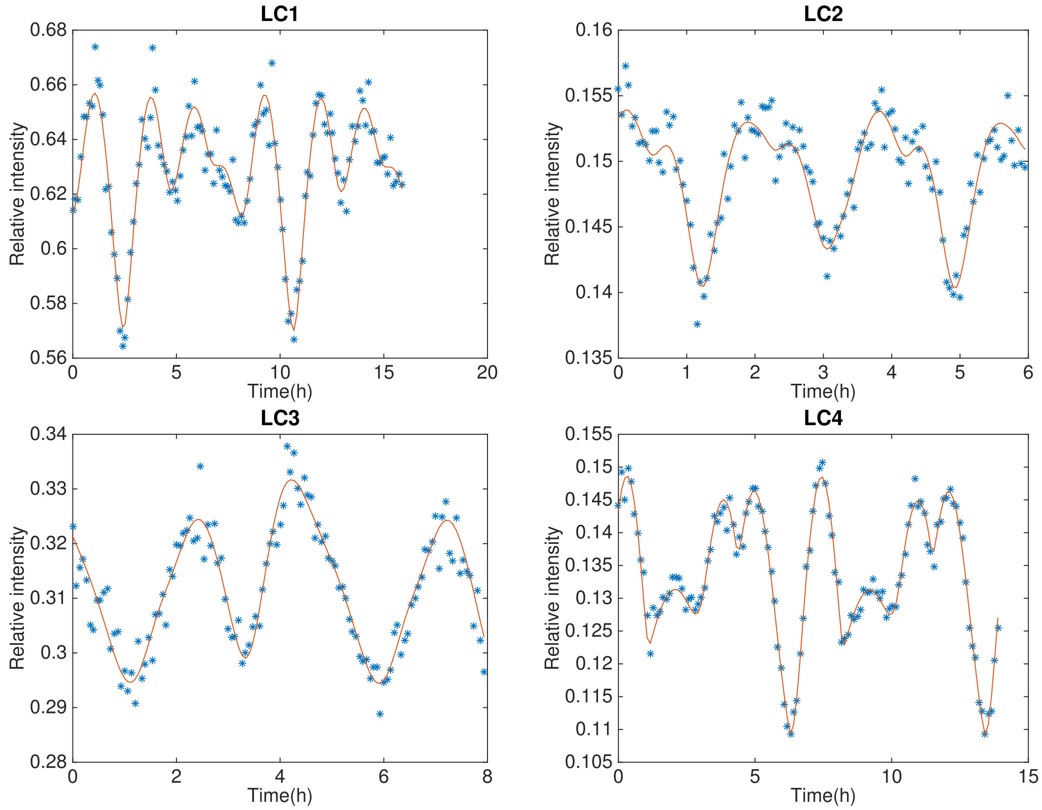

Figure 5. Synthetic lightcurves with Gaussian noise $N(0, 0.01)$.

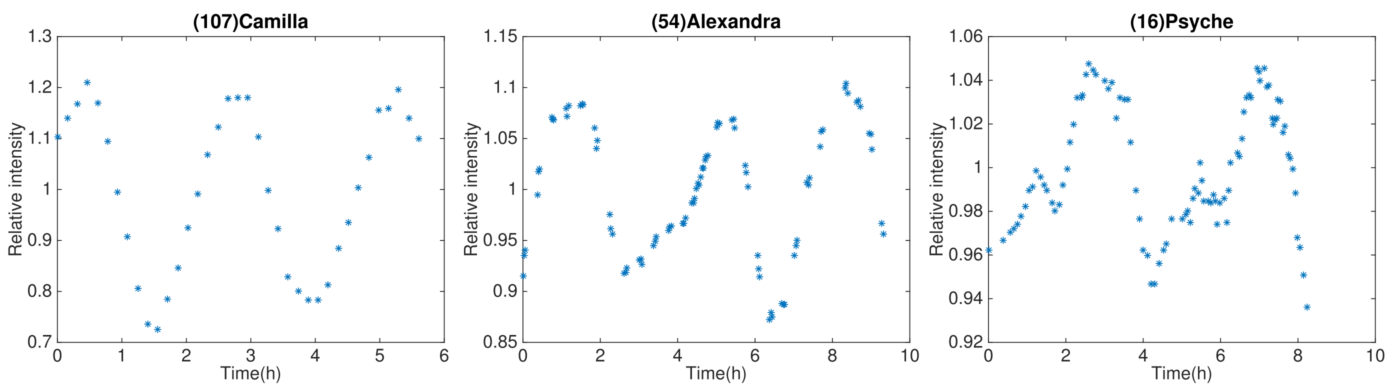

Figure 6. Lightcurves from real asteroids.

March 28 (Higgins & Warner 2009), and 1970 December 5 (Tedesco & Taylor 1985), shown in Figure 6.

By adopting the proposed hybrid method to these observed lightcurves as shown in Figure 6, the best-fit rotational periods are obtained and listed in Table 3. In Table 3, the error estimation for the period is added: first, a 0.1% random Gaussian noise is added to the obtained optimal period when the other optimal parameters are fixed, and this step is repeated 1000 times. Then, by minimizing the χ^2 of the 1000 set of parameters, a new optimal period can be obtained. Finally, a Gaussian fitting method is used to estimate the error range. Figure 7 shows the convergence process of searching the results for the three asteroids. It is obvious that the convergence speed of the proposed hybrid method for real asteroids is also very fast. Especially for the case of (54)Alexandra, even though the initial value of period is set to 19 hr, far away from the true value, the method can still converge to the true period after two generations. The feature of global optimization from the GA method can guarantee the convergence speed in searching the parameters using hybrid method. The fusion strategy of GA

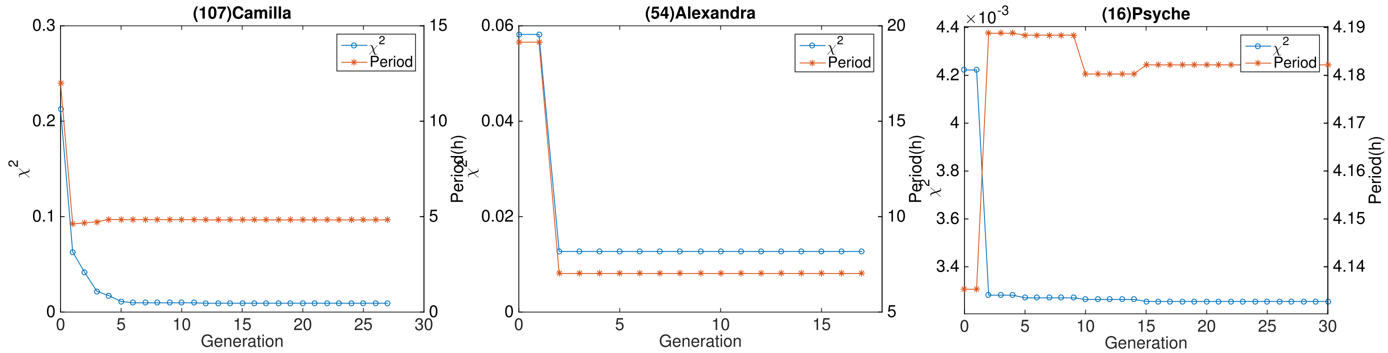

Figure 7. Convergence processes for real asteroids.

and LM can reduce the total computational cost. The time costs for inverting the three lightcurves are 19.62 minutes, 44.69 minutes and 56.98 minutes, respectively.

Furthermore, we have made the applications to lightcurves from more real asteroids, including the observation data on 1970 December 13 for (243) Ida (Mottola et al. 1994), 1984 March 9 for (125) Liberatrix (di Martino 1986), 1958 January 13 for (44) Nysa (Gehrels & Owings 1962), 2009 February 4 for (13) Egeria and 1973 December 16 for (7) Iris (Taylor 1977). The derived rotational periods are listed in Table 3. In comparison to the published results derived by the other works from DAMIT website, where the precision is not given (Kaasalainen et al. 2002; Torppa et al. 2003; Delbo & Tanga 2007; Ďurech et al. 2007, 2011; Warner et al. 2008; Polishook 2009; Hanuš et al. 2011, 2013, 2017; Viikinkoski et al. 2018; Vernazza et al. 2021), also listed in the table, the results by the hybrid method are consistent with the other known results. For the case of (7) Iris, the derived period is slightly deviated from the other ones in DAMIT. It should be noted that the result listed in DAMIT is a mean value inverted from many lightcurves observed for about tens of years, while in this experiment we only obtain the period from one individual lightcurve for the sake of quick calculations. Then there will be a deviation between the two results. In addition, the period in DAMIT is also combined with new observation data, which makes the results change.

4.3. Application to Real Asteroids with Sparse Observations

In the previous experiments, the proposed hybrid method is applied to the lightcurves observed in one apparition and the results are consistent with the published results by others. In the hybrid method and the original LM-based inverse process, the shape model is based on the Cellinoid shape, which consists of eight octants from ellipsoids. This shape is asymmetric while having simple representation using six semi-axes. As an intermediate approximation between the triaxial ellipsoid with three parameters and the convex shape model with more than

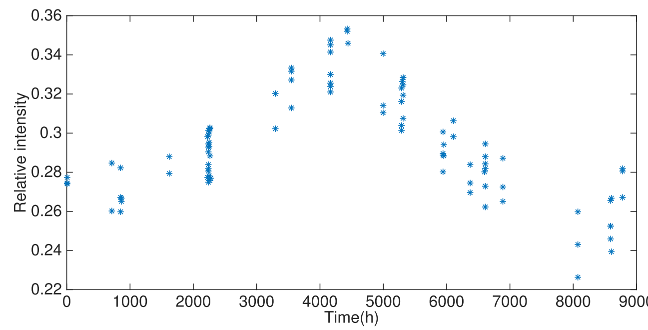

Figure 8. Synthetic data with sparse observations (the parameters are: $a_1 = 1.00$, $a_2 = 0.62$, $b_1 = 0.99$, $b_2 = 0.49$, $c_1 = 0.70$, $c_2 = 0.68$, $\lambda = 64$, $\beta = -58$, $P = 4.6$, $\Phi_0 = 194$, $K = -0.0023$, $B = 0.34$, $\gamma = 0.12$).

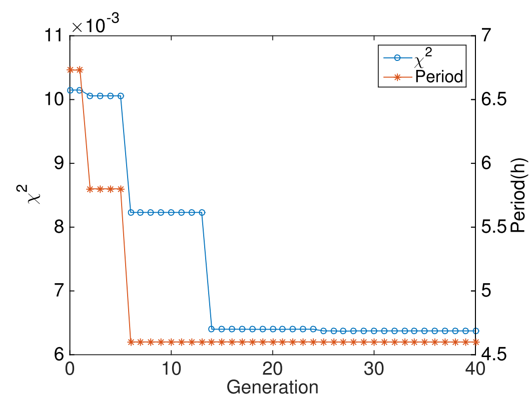

Figure 9. Convergence process of the hybrid method.

50 parameters, the Cellinoid shape model can perform well in simulating both dense observations and sparse observations, especially the latter ones, which are now widely collected from some space-based observations such as Gaia (Tanga et al. 2016) and ground-based sky survey program, such as PTF (Palomar Transient Factory; Waszczak et al. 2015) and SDSS (Sloan Digital Sky Survey; Ivezic et al. 2001). Lu et al. (2016)

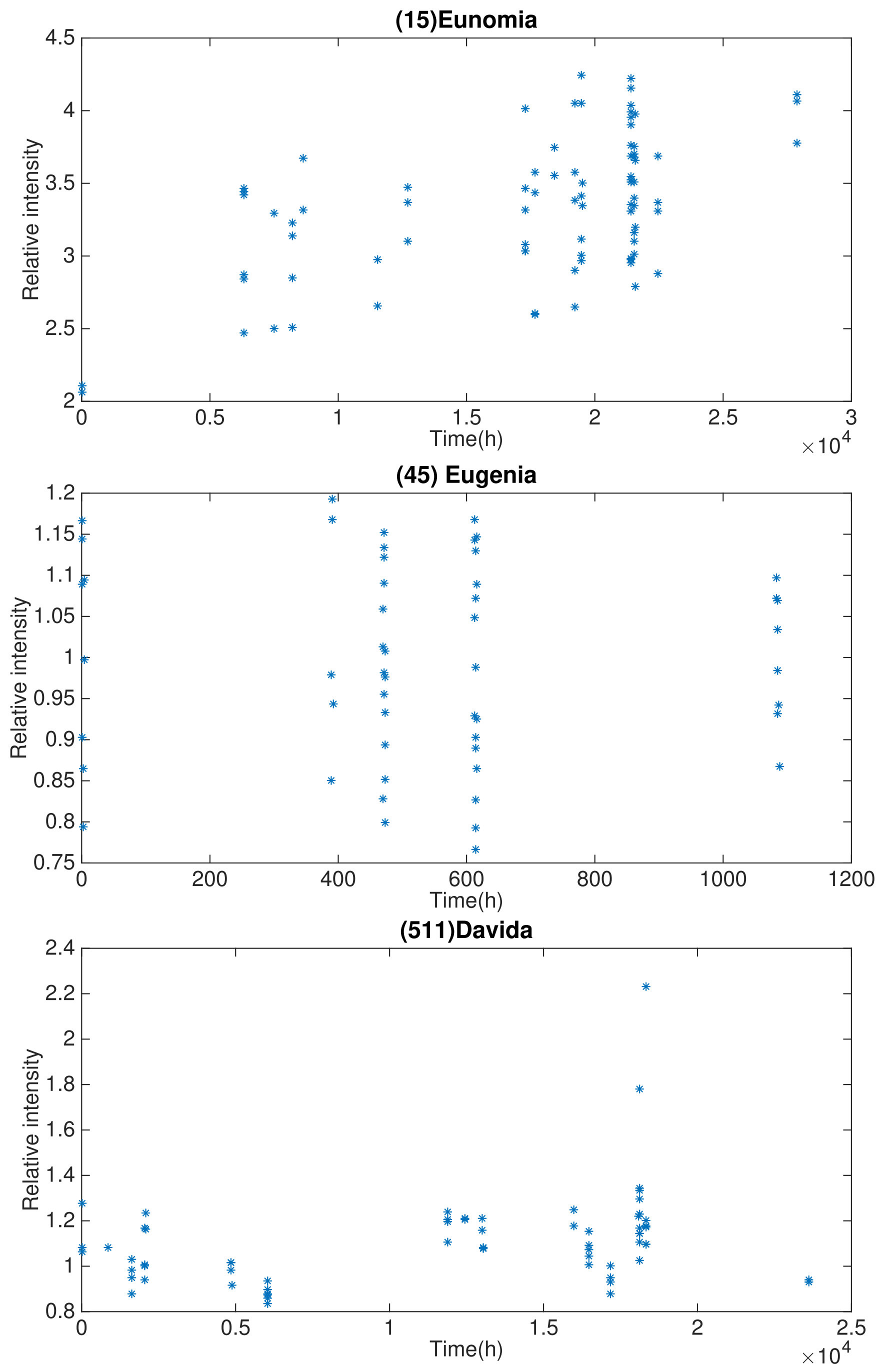

Figure 10. Collected sparse observations for (15) Eunomia, (45) Eugenia and (511) Davida.

has investigated the application of Cellinoid shape model to the sparse observations from the Hipparcos satellite. Here we employ the proposed hybrid method to the sparse observations to show its performance in handling these type data and extend its scope of applications.

First, as shown in Figure 8, a synthetic data set of sparse observations based on the specified parameters is generated, then by applying the proposed hybrid method the rotational period is searched and its convergence process is plotted in Figure 9.

In view of the large observation time span for sparse data, the population of the GA is expanded to 50. Additionally, as described by Warner et al. (2009), most asteroids located in the main belt have the rotational periods distributed between 2.2 hr

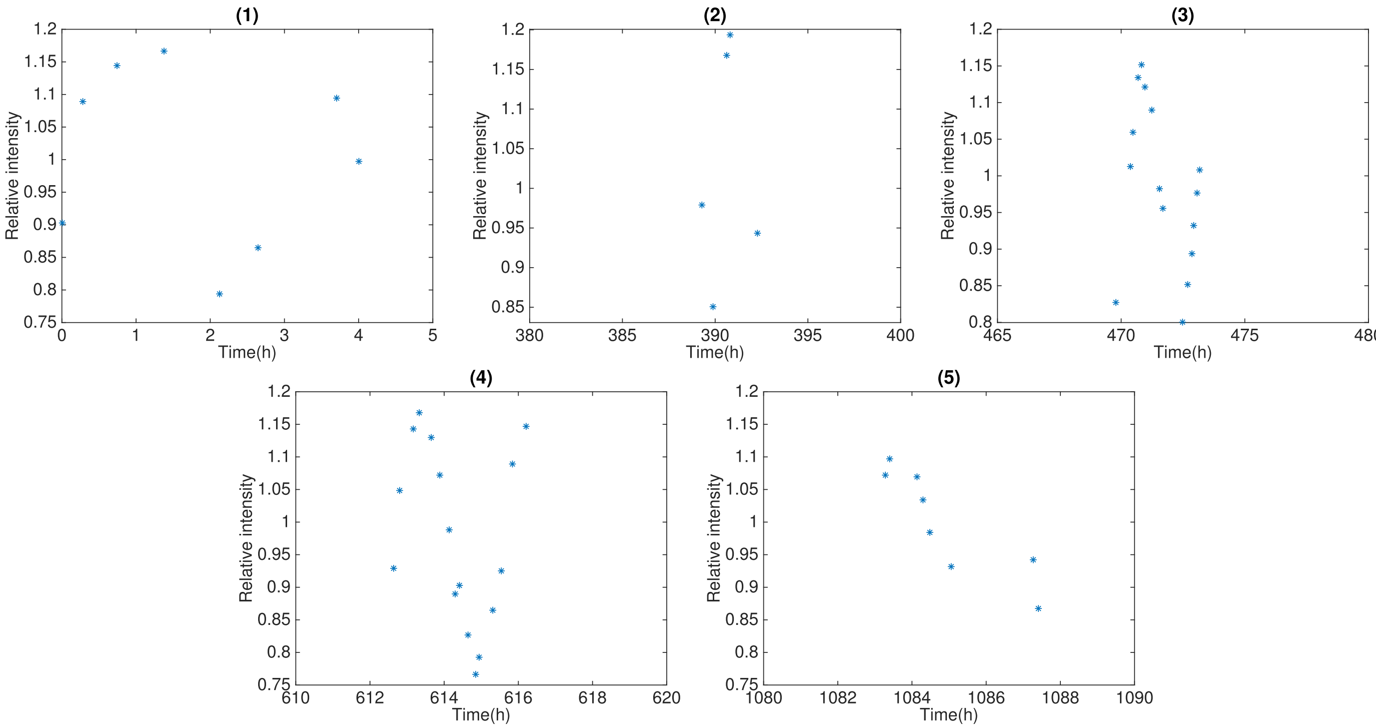

Figure 11. Sparse observations for (45) Eugenia.

Table 3
Derived Periods by the Hybrid Method for Real Asteroids

Asteroids	DAMIT/(hr)	$P_{G\&L}$/(hr)
(243)Ida	$P_1 = 4.633633$, $P_2 = 4.633632$	4.630389 ± 0.000667
(125)Liberatrix	$P_1 = 3.968199$	3.969400 ± 0.000429
(107)Camilla	$P_1 = 4.843928$	4.846091 ± 0.000826
(54)Alexandra	$P_1 = 7.022641$, $P_2 = 7.02264$	7.021639 ± 0.000301
(44)Nysa	$P_1 = 6.421417$	6.436159 ± 0.000979
(16)Psyche	$P_1 = 4.196948$	4.196426 ± 0.000248
(13)Egeria	$P_1 = 7.046671$, $P_2 = 7.046665$	7.045911 ± 0.000882
(7)Iris	$P_1 = 7.138843$, $P_2 = 7.138844$	7.115043 ± 0.000982

and 10 hr and the 2.2 hr is also called the spin-barrier. The selection interval for the period variable is therefore set to be [2, 10]. It should be noticed that in practice this interval could be extended to a larger one, like [1, 20] for better searching the accurate solutions. The derived period by the hybrid algorithm is 4.600172 hr with the residual χ^2 is 6.373×10^{-3}, which is almost the same as the preset period 4.6 hr. The convergence process in Figure 9 shows that the inverse process of proposed hybrid method can find the correct solution after about 15 generations.

With the verification of the proposed hybrid method in sparse data, we attempt to apply it to the sparse observations from real asteroids, (15) Eunomia, (45) Eugenia and (511) Davida. As shown in Figure 10, the collected sparse data were respectively observed from 1989 December 22 to 1993 February 26 for (15) Eunomia, from 1984 November 2 to 1984 December 17 for (45) Eugenia, and from 1990 June 3 to 1993 February 11 for (511) Davida (Lagerkvist et al. 1995; Weidenschilling et al. 1987; Taylor et al. 1988). Furthermore, Figure 11 demonstrates all the observations applied in this experiment for (45) Eugenia. Based on these sparse data from real asteroids, the proposed hybrid method is employed to derive their rotational periods and the results are listed in Table 4. In comparison to the results derived in other publications, it can be found that the hybrid method can perform well in obtaining the rotational period from the sparse observation data (Kaasalainen et al. 2002; Torppa et al. 2003; Hanuš et al. 2013; Nathues et al. 2015; Viikinkoski et al. 2017; Vernazza et al. 2021).

Table 4
Derived Periods by the Hybrid Method from Sparse Observations

Asteroids	DAMIT/(hr)	$P_{G\&L}$/(hr)
(15) Eunomia	$P_1 = 6.082753$, $P_2 = 6.082752$, $P_3 = 6.082754$	6.082949 ± 0.000913
(45) Eugenia	$P_1 = 5.699152$, $P_2 = 5.699152$	5.698331 ± 0.000208
(511) Davida	$P_1 = 5.129363$, $P_2 = 5.129364$, $P_3 = 5.129365$	5.123225 ± 0.005157

5. Conclusions

The photometric inversion process based on the shape model is commonly used to derive the physical parameters for asteroids from the observation data. Compared to the Fourier-based methods, which can give an estimate of the rotational period, the inversion process could obtain other results including the pole orientation and overall shape. Furthermore, they can even search the parameters based on some simple shape models such as the Cellinoid and triaxial ellipsoid shapes from sparse observations, not only lightcurves like Fourier methods.

However, the inverse process is very time-consuming because they have to calculate the simulated brightness based on the surface discretization and some gradient-based optimization methods. In this article, a hybrid of the GA and LM algorithms based on the Cellinoid shape model is proposed for accelerating the inversion process. Numerical experiments with synthetic observation data show that this hybrid method, compared with the single LM algorithm, greatly reduces the computational cost while preserving the accuracy of derived results. Furthermore, the presented method is applied to real asteroids and the obtained rotational periods using one apparition lightcurve and sparse data are both close to the results obtained by other authors. Different from the usual individual algorithm, or the idea of exploiting two algorithms one after another, we integrate the LM algorithm into the evolution process of GA as a whole process, fusing them into one algorithm for the inversion. The hybrid strategy can largely improve the efficiency of searching the best-fit physical parameters while keeping the accuracy.

Acknowledgments

The authors sincerely thank the anonymous reviewers for their constructive comments that help greatly improve the manuscript. This work is funded by the grant from the Macao Young Scholars Program (Project code: AM201920), the National Natural Science Foundation of China (NSFC, grant No. E11903085). X.-P. Lu is funded by the Science and Technology Development Fund, Macau SAR (File Nos. 0073/ 2019/A2 & 0096/2022/A). X. Zhang is supported by the Science and Technology Development Fund, Macau SAR (File No. 0042/ 2018/A2). H.-B. Zhao is supported by the B-type Strategic Priority Program of CAS (Grant No. XDB41000000), the NSFC (Grant Nos. 62227901 & 11633009), Space debris and NEO research project (Nos. KJSP2020020204 & KJSP2020020102) and Minor Planet Foundation.

References

Cellino, A., Hestroffer, D., Tanga, P., Mottola, S., & Dell'Oro, A. 2009, A&A, 506, 935
Cellino, A., Zappalà, V., & Farinella, P. 1989, Icar, 78, 298
Cho, D., & Zhang, B. 2004, LNCS, 3242, 212
De Jong, K. 1975, PhD thesis, Univ. of Michigan, Ann Arbor Analysis of Behavior of a Class of Genetic Adaptive Systems
Delbo, M., & Tanga, P. 2007, P&SS, 57, 259
di Martino, M. 1986, in Asteroids, Comets, Meteors II: Proc. Int. Meeting (Uppsala, Sweden: Astronomiska Observatoriet), 81
Ďurech, J., Kaasalainen, M., Herald, D., et al. 2011, Icar, 214, 652
Ďurech, J., Kaasalainen, M., Marciniak, A., et al. 2007, A&A, 465, 331
Gehrels, T., & Owings, D. 1962, AJ, 135, 906
Gen, M., & Cheng, R. 1996, Genetic Algorithms and Engineering Design No. 1st (New York: Wiley)
Hanuš, J., Ďurech, J., Brož, B., et al. 2011, A&A, 530, A134
Hanuš, J., Ďurech, J., Oszkiewicz, D., et al. 2016, A&A, 586, A108
Hanuš, J., Marchis, F., & Ďurech, J. 2013, Icar, 226, 1045
Hanuš, J., Viikinkoski, M., Marchis, F., et al. 2017, A&A, 601, A114
Higgins, D., & Warner, B. D. 2009, MPBu, 36, 159
Holland, J. 1975, Adaptation in Natural and Artificial Systems (Ann Arbor: Univ. Michigan Press)
Ivezic, Z., Tabachnik, S., Rafikov, R., et al. 2001, AJ, 122, 2749
Kaasalainen, M., Lamberg, L., & Lumme, K. 1992a, A&A, 259, 333
Kaasalainen, M., Lamberg, L., Lumme, K., & Bowell, E. 1992b, A&A, 259, 218
Kaasalainen, M., & Torppa, J. 2001, Icar, 153, 24
Kaasalainen, M., Torppa, J., & Muinonen, K. 2001, Icar, 153, 37
Kaasalainen, M., Torppa, J., & Piironen, J. 2002, Icar, 159, 369
Kaasalainen, S., Kaasalainen, M., & Piironen, J. 2005, A&A, 440, 1177
Karttunen, H., & Bowell, E. 1989, A&A, 208, 320
Lagerkvist, C., Erikson, A., Debehogne, H., et al. 1995, A&AS, 113, 115
Li, X., Xin, W., & Xiong, Y. 2019, AdSpR, 63, 999
Lu, X., Cellino, A., Hestroffer, D., & Ip, W. 2016, Icar, 267, 24
Lu, X., Zhao, H., & You, Z. 2013, A&A, 13, 465
Lu, X., Zhao, H., & You, Z. 2014, EM&P, 112, 73
Lu, X. I. W., Huang, X., & Zhao, H. 2017, P&SS, 135, 74
Lumme, K., & Bowell, E. 1981a, AJ, 86, 1694
Lumme, K., & Bowell, E. 1981b, AJ, 86, 1705
Marquardt, D. 1963, JSTOR, 11, 443
Mottola, S., Gonano-Beurer, M., Green, S., et al. 1994, P&SS, 42, 21
Muinonen, K., & Lumme, K. 2015, A&A, 584, A23
Muinonen, K., Piironen, J., Kaasalainen, S., & Cellino, A. 2002, MmSAI, 73, 716
Muinonen, K., Wilkman, O., Cellino, A., et al. 2015, P&SS, 118, 227
Nathues, A., Mottola, S., Kaasalainen, M., & Neukum, G. 2005, Icar, 175, 452
Peña, J., Robles, V., Larrañaga, P., et al. 2004, LNCS, 3029, 361
Polishook, D. 2009, MPBu, 36, 119
Press, W., Flannery, B., Teukolsky, S., & Vetterling, W. 1992, A Numerical Recipes: The Art of Scientific Computing No. 2nd (Cambridge: Cambridge Univ. Press)
Russell, H. 1906, AJ, 24, 1
Surdej, A., & Surde, J. 1978, A&A, 66, 131
Tanga, P., Mignard, F., Oro, A., et al. 2016, P&SS, 123, 87
Taylor, R. 1977, AJ, 82, 441
Taylor, R., Birch, P., Pospieszalska-Surdej, A., & Surdej, J. 1988, Icar, 73, 314
Tedesco, E., & Taylor, R. 1985, Icar, 61, 241
Torppa, J., Kaasalainen, M., Michałowski, T., et al. 2003, Icar, 164, 346
Vernazza, P., Ferrais, M., Jorda, L., et al. 2021, A&A, 654, 56
Viikinkoski, M., Hanuš, J., Kaasalainen, M., et al. 2017, A&A, 607, 117
Viikinkoski, M., Vernazza, P., Hanus, J., et al. 2018, A&A, 619, L3
Warner, B., Harris, A., & Pravec, P. 2009, Icar, 202, 134
Warner, B., Ďurech, J., Fauerbach, M., & Marks, S. 2008, MPBu, 35, 167
Waszczak, A., Chang, C., Ofek, E., et al. 2015, AJ, 150, 75
Weidenschilling, S., Chapman, C., Davis, D., et al. 1987, Icar, 70, 190